ELSEVIER

Biophysical Chemistry 122 (2006) 90–100

Biophysical Chemistry

http://www.elsevier.com/locate/biophyschem

A hand-over-hand diffusing model for myosin-VI molecular motors

Ping Xie *, Shuo-Xing Dou, Peng-Ye Wang

Laboratory of Soft Matter Physics, Beijing National Laboratory for Condensed Matter Physics, Institute of Physics, Chinese Academy of Sciences, Beijing 100080, China

Received 25 November 2005; received in revised form 20 February 2006; accepted 21 February 2006
Available online 27 March 2006

Abstract

Single molecules of dimeric myosin-VI have been demonstrated to be able to move processively towards the pointed end of actin filament with a mean step size of ~ 36 nm. Here we present a hand-over-hand diffusing mechanism for this unidirectional movement. Based on this mechanism, its dynamical behaviors such as the step-size distribution, dwell-time distributions and mean dwell time at various ATP and ADP concentrations and under various loads are studied in detail. The calculated results show good agreement with previous experimental results. The processive movement of mutant myosin-V with its neck domains truncated to only one IQ motif can also be explained by using this hand-over-hand diffusing model.

Keywords: Myosin-VI; Model; Dynamics; Molecular motor

1. Introduction

Myosin-VI functions in several critical intracellular processes such as vesicular membrane traffic, cell migration, maintenance of stereocilia, and mitosis [1–5]. It was the first myosin shown to move in the opposite direction on actin filaments as compared to myosin-II [6]. It is recently discovered that both expressed full-length and native myosin-VI are monomeric [7]. However, single molecules of constructed dimeric myosin-VI have been demonstrated to be able to move processively along actin filament [6,8,9]. Like myosin-V, the dimeric form of myosin-VI is composed of two heavy chains, each consisting of a head domain and an α-helical coiled coil. The head domain of myosin-VI contains two inserts that are unique within the myosin superfamily, with the first one near the nucleotide-binding pocket in the motor domain and the second one between the converter and the IQ motif in the neck domain [6,10,11]. As the neck domain has only two calmodulins bound to insert 2 and the IQ motif, its length is much shorter than that of myosin-V that contains 6 IQ motifs bound with 6 calmodulins. Nevertheless, it also moves stepwise along actin with a mean step size of ~36 nm, similar to myosin-V. One of the distinct features of myosin-VI from other myosins is that it moves processively towards the pointed (minus) end of an actin filament [6,8–10].

By using different experimental methods such as biochemical, biophysical, and single-molecule approaches, many aspects of the behaviors of myosin-VI have been gradually elucidated. In particular, its dwell-time distributions and mean dwell time at various ATP and ADP concentrations and under various loads have been systematically and elaborately determined by using optical trapping nanometry [8,9,12,13].

Nevertheless, the microscopic mechanism of myosin-VI has not been completely determined yet. Since myosin-VI has very short neck domains (lever arms), which cannot span the size of ~ 36 nm, it is difficult to imagine how myosin-VI can walk along actin in a manner like myosin-V. A modification of the lever-arm model has been proposed that predicts a step consisting of a working stroke of the short lever arm followed by a diffusive search. The working stroke provides part of the step size and imparts directionality while the diffusive search allows the leading head to find further actin-binding sites [8,12,14–16]. This proposal postulates that the region immediately following the IQ motif (the proximal tail) might come apart to form flexible linker during the motile cycle of myosin-

* Corresponding author. Tel.: +86 10 82649568; fax: +86 10 82640224.
E-mail address: pxie@aphy.iphy.ac.cn (P. Xie).

0301-4622/$ - see front matter © 2006 Elsevier B.V. All rights reserved.
doi:10.1016/j.bpc.2006.02.010

VI on actin. This model gives that myosin-VI walks in a hand-over-hand manner, which is much like kinesin. An alternate model based on biased Brownian motion has been proposed, where the movement of myosin-VI is realized by biased thermal diffusion of its heads along actin [9]. Thus the short neck length does not affect the step size and myosin-VI can still move ~36 nm in one step.

In this work, based on our previous work [17], we present a new hand-over-hand diffusing model for the processive movement of myosin-VI by incorporating the nucleotide-state-dependent orientation of the neck domain relative to the motor domain. In this model, it is postulated that during the dwell period only one head binds to actin, while during the stepping period both heads are detached from actin. Based on this model we study the dynamical behaviors of single myosin-VI molecules. The theoretical results such as dwell-time distributions and mean dwell time at various ATP and ADP concentrations and under various loads show good quantitative agreement with available experimental results.

2. Interaction of a myosin head with actin

From experimental evidences [18–22], it is known that the interaction between a myosin head and actin depends on its nucleotide state. Generally, in ADP state, and ensuing release of ADP, i.e., in nucleotide-free state, the myosin head has a strong interaction with actin. In ATP and ADP.Pi states, the myosin head has a weak interaction with actin. In detail, we describe the evolution of the interaction force between actin and the myosin head after ATP binding as follows. Similar to that adopted for kinesins [23], immediately after ATP binding, the binding affinity for myosin of the several local binding sites of actin around which the head is binding becomes much weaker than the other binding sites. The distribution of the binding affinity of actin for myosin is schematically shown in Fig. 1(a), where the binding site with the highest affinity is shown in red and as the colour becomes lighter the affinity becomes weaker. Note that the binding site of actin with the least azimuthal distortion, i.e., the binding site on the side where the myosin motor domain lies, has the highest affinity and, as the binding site rotates away from this site, the affinity becomes weak [24]. After a period of time, t_r, the affinities for myosin of the local binding sites of actin relax to the normal values. The distribution of the binding affinity of actin for myosin is now schematically shown in Fig. 1(b).

Here we give an explanation to the temporal evolution of the binding affinity of actin for myosin (Fig. 1(a) and (b)) as follows. The ATP binding induces the conformational change in the actin-binding site of myosin motor domain, i.e., the conformational change from the closed to open cleft between the 50 kDa subdomains [20], which results in its weak interaction with actin. On the other hand, it has been acknowledged that the strong interaction of myosin with actin results in a structural change to the local actin monomer. As further evidenced by Prochniewicz et al. [25], this effect of myosin-induced conformational change of the single actin monomer may propagate to a group of four to five nearby

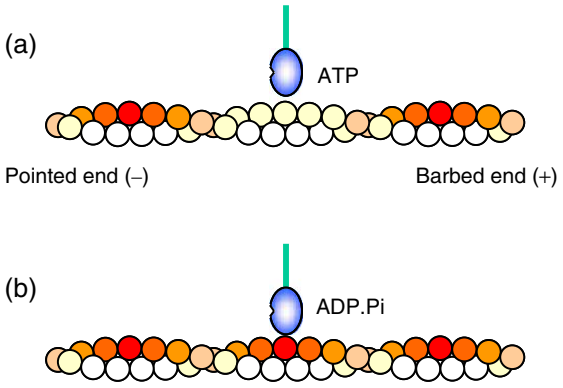

Fig. 1. Schematic illustration of the distribution of the binding affinity of actin for myosin. The binding site with the highest affinity is shown in red and as the colour becomes lighter the affinity becomes weaker. Note that the binding site of actin on the side where the myosin motor domain lies has the highest affinity and, as the binding site rotates away from this site, the affinity becomes weak. (a) Immediately after ATP binding, myosin is detached from actin. The affinity for myosin of the several local binding sites of actin nearby the monomer where the myosin has just bound is very low due to conformational changes induced by the strong interaction with myosin (see the text). (b) After a period of t_r, the affinities of the several local binding sites nearby the monomer where myosin has just bound relax to their normal values. (For interpretation of the references to colour in this figure legend, the reader is referred to the web version of this article.)

monomers. Thus it is expected that, after ATP-binding-induced detachment of the bound myosin, the conformations of the several local actin monomers should still be different from others. Therefore, it is reasonable to assume that the ATP–myosin complex has weaker interactions with the several local binding sites of actin than those with other unaffected sites. After a period of time, t_r, the conformations of the several local binding sites (or monomers) of actin around which the myosin has just been bound relax to their normal conformations and thus the interactions of the ATP–myosin with these binding sites of actin become the same as those with other unaffected binding sites. It is mentioned that, although it had been acknowledged that the strong interaction of myosin with actin results in the structural change to actin, the role that such structural change would play in actomyosin-based motility remained undefined [22]. As we will show in Section 3, it is based on this structure-change-induced reduction of the interaction affinity between the motor domain and the local binding sites that myosin-VI moves processively with a 1:1 mechanochemical coupling.

It is interesting to note that the kinetic analysis [26] indicated that the affinity for actin of myosin in ATP state is at least 20-fold higher than that of myosin in ADP.Pi state. Then it is a very puzzling phenomenon that ATP binding to nucleotide-free actomyosin induces the detachment of myosin from actin, while ADP.Pi myosin can bind to actin. However, based on our discussion of the temporal evolution of the binding affinity of actin for myosin as schematically shown in Fig. 1, this phenomenon that ATP binding to the nucleotide-free actomyosin induces the detachment of myosin from actin can be readily explained. On the other hand, when the preincubated solution of myosin and ATP is mixed with actin, as done in experiment of

Ref. [26], the ATP myosin head has a higher affinity for actin, because actin is now not affected by myosin.

3. Hand-over-hand diffusing mechanism

It has been known that the relative orientation of the neck domain with respect to the motor domain of a myosin head depends on its nucleotide state. In general, in weak actin-bound ATP and ADP.Pi states the myosin head has a similar conformation, which is called pre-power-stroke conformation. In strong actin-bound ADP and nucleotide-free states the myosin head has another similar conformation, which is called post-power-stroke conformation. Here we neglect the possible difference between the ADP conformation and the nucleotide-free conformation. The structure of a myosin-VI head revealed the post-power-stroke conformation as shown in Fig. 2(a) [11]. Note that the relative orientation of its neck domain to the motor domain is in opposite direction to that of myosin-II and myosin-V [27]. This different relative orientation may be due to the presence of the extra insert 2 in the myosin-VI head [11]. The EM images of full length myosin-VI in ADP.Pi state show the neck domain in what would be a roughly perpendicular orientation to the actin filament [7]. It is thus assumed that the pre-power-stroke conformation in ATP and ADP.Pi states is as shown in Fig. 2(b). Note that the motor domain of myosin-VI should also bind to actin in the same fixed orientation as that of myosin-V [17], as shown in Fig. 2.

When myosin-VI is dimerized, from the conformation of its single-headed counterpart (Fig. 2(a)), it is reasonable to assume that the equilibrium conformation of the dimer, with both heads in nucleotide-free state in the absence of actin, should have the form as shown in Fig. 3(a), with the relative orientation of the two heads being nearly mirror symmetrical. It is argued here that the residue segments connecting the neck domains and the coiled coil behave elastically, with a non-zero bending elastic stiffness, rather than as a generally believed completely flexible element of nearly zero bending elastic stiffness (i.e., the residue segment being a "hinge point" around which the neck domain can rotate freely).

This argument is in agreement with the recent experimental result by using single-molecule nanomechanics method for myosin-II [28], where the bending stiffness of the "hinge points" or residue segments that connect the neck domains and the coiled coils was estimated to be 2.5 k_BT/rad. Furthermore, based on this argument, it is expected that the non-zero bendable stiffness of the "hinge points" or the residue segments would keep the two heads of myosin-VI fluctuating, due to noise, around their equilibrium orientations in a limited range.

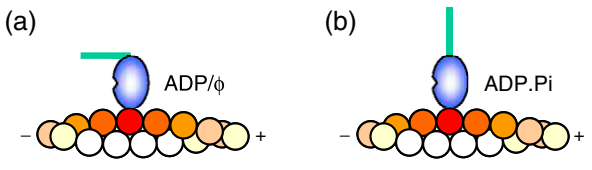

Fig. 2. The conformations of a single myosin-VI head in (a) post-power-stroke ADP or nucleotide-free (ϕ) state and (b) pre-power-stroke ATP or ADP.Pi state.

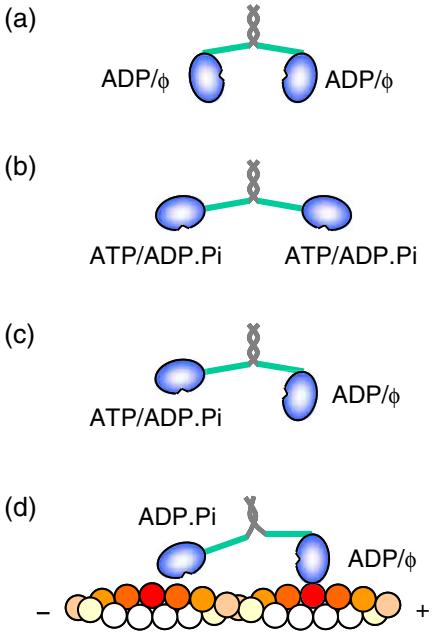

Fig. 3. The equilibrium conformations of dimeric myosin-VI with (a) both heads in ADP or nucleotide-free (ϕ) states, (b) both heads in ATP or ADP.Pi states, and (c) one head in ADP or nucleotide-free (ϕ) state and the other one in ATP or ADP.Pi state. (d) The conformation of myosin-VI with one head in ADP or nucleotide-free (ϕ) state binding to actin and the other head in ADP.Pi state.

This is also in agreement with the earlier experimental results by using phosphorescence anisotropy decay measurements for conventional myosin-II in Ref. [29]: myosin heads have a favored orientation with a relatively small angular range with semi-angle of about 12.5° under relaxing conditions. In addition, by using the same method, Ishiwata et al. [30] have shown that a myosin-II in solution consists of two components of rotation in cones with semi-angles of about 32° and 47°, respectively. The former component was attributed to the rotation of the myosin head (the motor domain and the neck domain) relative to the tail [30]. This means that the myosin head can only rotate "freely" around the "hinge point" or residue segment in a limited range of 32° semi-angle. However, if this "hinge point" or residue segment is a flexible element of nearly zero bendable stiffness, which means a free rotation of the myosin head around the "hinge point", it would be expected that the rotation of the myosin head to the tail should be in a wider range of up to 90° in semi-angle under the experimental condition in Ref. [30]. Due to the non-zero stiffness, the thermal noise induces the rotation in the range with the semi-angle of only 32° around its equilibrium orientation. Thus, after myosin-VI is dimerized, it is similarly expected that the non-zero bending stiffness of the two "hinge points" or residue segments connecting the necks and the coiled coils would keep its two heads fluctuating in a limited range around their equilibrium orientations, as shown in Fig. 2. The favored orientations with a limited angular range for the two heads of other dimeric myosins are also supported by various EM observations of myosin conformations in the absence of actin [31–33]. Furthermore, as stated in Ref. [34], the two heads of a homodimeric molecular motor emerge from a coiled coil of α-

helices, each helix extending into a neck. Because the coiled coil is twofold symmetric, as confirmed for kinesin [35] and myosin [36], the two identical motor domains are also arranged, basically, in the same twofold symmetry, i.e., the two motor domains would be oriented in nearly opposite directions.

When ATP binds to both heads, from Figs. 2(b) and 3(a) we deduce that the equilibrium conformation of the dimer has the form as shown in Fig. 3(b). After hydrolysis of ATP to ADP.Pi, the equilibrium conformation still shows the same form. When one head is in ADP/ϕ state and the other one in ATP/ADP.Pi state, the conformation is as shown in Fig. 3(c).

Considering that one head in ADP or nucleotide-free state binds strongly to actin and the other head in ADP.Pi state. Since the neck domains are short and the region immediately following the IQ motif (the proximal tail) should have non-zero stretchable elastic stiffness, it is thus less probable for the neck domain to bend enough and for the coiled coil to come apart far enough (>24 nm) for the ADP.Pi head to bind actin in the same fixed orientation.[1] Thus, in rigor state with one head binding strongly to actin in ADP or nucleotide-free state, the other head in ATP or ADP.Pi state is most probably unable to bind to actin, with the conformation as shown in Fig. 3(d). This feature of rigor state for myosin-VI is different from that for myosin-V, where, because each myosin-V head has a long neck domain, containing 6 IQ motifs plus 6 light chains, the long neck domain can be bended elastically [37] to make the two heads (one in ADP or nucleotide-free state and the other one in ADP.Pi state) bind simultaneously to actin in equivalent orientations. Since the region immediately following the IQ motif may have a low probability of forming a stable coiled coil [36], the distance between the two motor domains in Fig. 3(c) may, due to the binding affinity of the binding sites of actin near the unbound head, vary in a range of about 25–33 nm, where we have taken the neck length as ~ 10 nm, the motor domain size as ~10 nm and the separation between the adjacent ends of the two neck domains as 0–8 nm. The mean inter-head distance of ~29 nm is consistent with the experimental result of ~29.3 nm [38].

Based on above discussion, we propose the model for processive movement of myosin-VI towards the pointed end (i.e., minus end) of actin as follows. We begin with one head in nucleotide-free state binding strongly to binding site (I) and the other head in ADP.Pi state being unbound to actin, as shown in Fig. 4(a). For convenience of writing, we call the head close to the pointed end of actin the leading head and that close to the barbed end the trailing head. Note that, in Fig. 4(a), the unbound leading head is positioned much nearer binding site (II) than binding site (I) of actin, where the actin-binding site of the unbound leading head is in a plane with the two binding sites (I) and (II), i.e., the binding sites (I) and (II) have the least

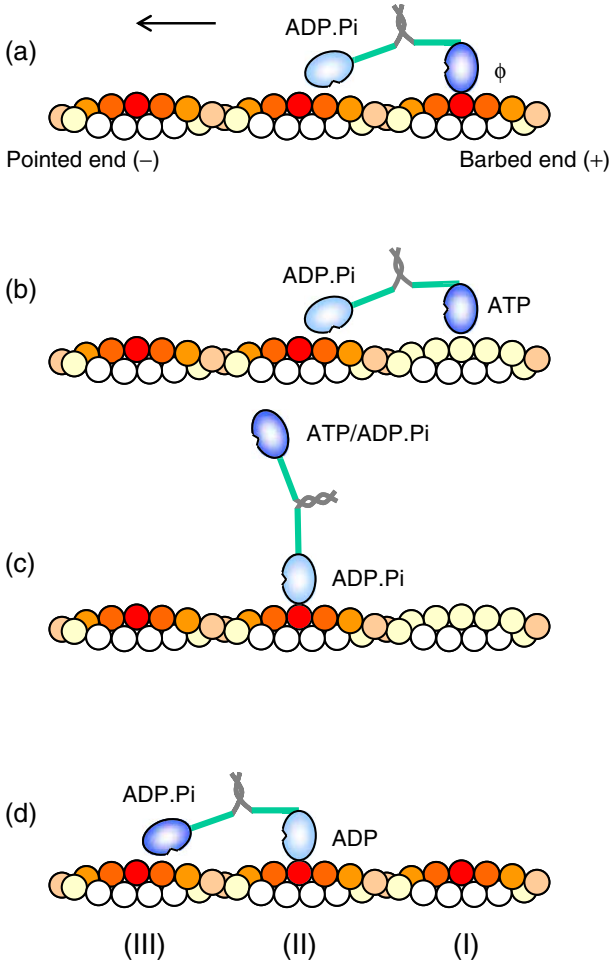

Fig. 4. Schematic illustrations of hand-over-hand diffusing mechanism for myosin-VI. (a) The trailing head (blue) in nucleotide-free (ϕ) state binds strongly to binding site (I) and the leading head (light blue) in ADP.Pi state is unbound to actin. (b) ATP binds to the trailing head (blue). (c) The leading head (light blue) binds to actin and, immediately, myosin-VI changes to its equilibrium conformation as shown in Fig. 3b. (d) After Pi release from the bound head (light blue), the rotation of its neck domain makes myosin-VI change to its new equilibrium conformation as shown in Fig. 3c. After ADP release from new trailing head (light blue), an ATPase cycle is completed with a mechanical step being made. (For interpretation of the references to colour in this figure legend, the reader is referred to the web version of this article.)

azimuthal distortion relative to the actin-binding site of the leading head. Thus there exists a net force, F_x, along actin pointed towards the pointed end on the unbound leading head. Upon ATP binding to the nucleotide-free bound trailing head, the interaction between the trailing head and the local binding sites of actin becomes much weak, as shown in Fig. 1(a), and thus the head is detached from actin, as shown in Fig. 3(b). Then due to F_x, the myosin has a larger probability to move towards the next binding site (II). As noted from Fig. 4(b), during the very short moving period with both heads detached from actin, besides the above-mentioned horizontal component F_x of the interaction force (e.g., the electrostatic force) between the leading head and actin monomers, there should also exist a perpendicular component pointed towards actin, F_y, of the electrostatic force, thus preventing myosin-VI to diffuse away from actin. Upon the leading head binding to the new binding

[1] If the coiled coil immediately following the IQ motif can come apart far enough (~24 nm), in the rigor state of myosin-V, with both heads in post-power-stroke conformations simultaneously binding to actin, the coiled coil should also come apart very far and the long neck domain of the leading head should remain, due to large bendable stiffness, nearly straight rather than curved as observed from EM by Walker et al. [48]. However, this conformation of myosin-V with the two neck ends near the coiled coil coming apart very far has never been observed by using EM.

site (II) of actin, as required by the equilibrium state (see Fig. 2), the conformation of the myosin immediately becomes that as shown in Fig. 3(c). After Pi release from the bound head, its neck domain is rotated to the post-power-stroke orientation, as shown in Fig. 4(d). When ADP is released from the new trailing head, the myosin-VI returns to the state as shown in Fig. 4(a), with a mechanical step from site (I) to site (II) being made in one ATPase cycle.

It is interesting to note that this moving behavior of myosin-VI is somewhat like a human running, with two heads simultaneously detached from the track during the moving period. This is in contrast to the walking behavior of myosin-V and conventional kinesin, where only one head is detached from the track during the moving period.

In the following, we will give quantitative descriptions to the dynamic behaviors of myosin-VI motors based on this model.

4. Step-size distribution

According to the mechanism presented in above section, the position nearby the binding site (II) in Fig. 4(b) where the leading head will bind after ATP binding to the trailing head is determined by both the position of the leading head in the previous rigor state (Fig. 4(a)) and the target function, $A(U)$, measured by Steffen et al. [39]. Thus, in this section we will use the experimental results for $A(U)$ in Ref. [39] to calculate the step-size distribution, where U represents the position of the binding site of actin, with origin ($U=0$) located at the binding site having the least azimuthal distortion relative to the actin-binding site of the myosin head.

The binding probability of a myosin head in the experiment of Ref. [39] was calculated by using the form

$$J(U,x)\propto\exp\left(-\frac{(U-x)^2}{2S^2}\right)A(U), \tag{1}$$

where $\exp(-(U-x)^2/(2S^2))$ is a Gaussian distribution describing thermally driven longitudinal fluctuations in the relative position between actin and myosin, with S being the standard deviation and x being the position of the myosin head. The target function $A(U)$ has the form

$$A(U)=\sum_{i=-N}^{N}\exp\left(-\frac{1}{2}\alpha\left(\pi\frac{U-id}{d}\right)^2\right), \tag{2}$$

where α is a parameter and $d=36$ nm is the half-repeat distance of actin. Using Eqs. (1) and (2) the measured histograms of the distributions of bound levels were fitted very well, with the fitted values of parameters as $S=13.5$ nm and $\alpha=3.7$ [39].

During the moving period of myosin-VI, according to our model the target function $A_M(U)$ in Fig. 4(b) and (c) approximately has the following form

$$A_M(U)=\sum_{i=-N}^{N}\exp\left(-\frac{1}{2}\alpha\left(\pi\frac{U-id}{d}\right)^2\right)-\exp\left(-\frac{1}{2}\alpha\left(\pi\frac{U}{d}\right)^2\right), \tag{3}$$

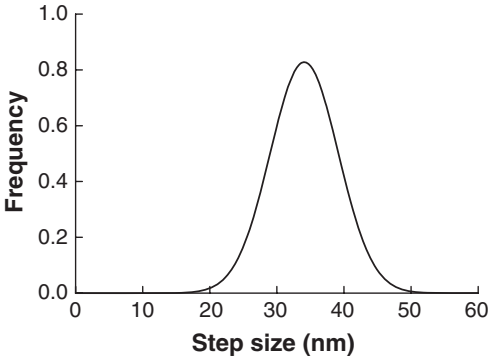

Fig. 5. Calculated step-size distribution using $D(U,x)\propto P(U,x)A_M(U)$ and Eqs. (3) and (4). The parameters used are $\alpha=3.7$ and $S=9.7$ nm.

where the position of the trailing head in the previous rigor state (Fig. 4(a)) is taken as $U=0$. The thermally driven longitudinal fluctuation in the position of the leading head relative to actin can be described by

$$P(U,x)=\frac{1}{\sqrt{\pi/2}S}\exp\left(-\frac{(U-x)^2}{2\times S^2}\right), \tag{4}$$

where x is the position of the actin-binding site of the leading head (i.e., the distance between the two actin-binding sites of the two heads in rigor state in Fig. 4(a)). From the conformation of myosin-VI in rigor state we approximately have the distance $x=29$ nm as estimated in Section 3. Using $D(U,x)\propto P(U,x)A_M(U)$ we calculate the step-size distribution $D(U,x)$ of myosin-VI, i.e., the distribution of the distance between the binding position of the leading head (Fig. 4(c)) and the position of the trailing head in previous rigor state (Fig. 4(a)), where we use $\alpha=3.7$ as measured in Ref. [39] and the standard deviation $S=9.7$ nm as obtained from Gaussian fitting of the measured inter-head distance in Ref. [38]. The result is shown in Fig. 5. The calculated result shows resemblance to the experimental ones [8,9]: The mean step size (~35 nm) is nearly the same as that for myosin-V, but with the step-size distribution being much wider than that for myosin-V [8]. The narrower step-size distribution of myosin-V is due to that the lengths of the neck domains are long enough for the free head to bind actin immediately after it reaching its equilibrium position [17].

5. Theoretical approach to kinetics

An ATPase cycling of a given myosin head is described by the following scheme $\mathrm{ADP}\underset{k_{-1}}{\overset{k_1}{\rightleftarrows}}\mathrm{ADP}^*\underset{k_{-2}}{\overset{k_2}{\rightleftarrows}}\mathrm{Empty}\underset{k_{-3}}{\overset{k_3}{\rightleftarrows}}\mathrm{ATP}\underset{k_{-4}}{\overset{k_4}{\rightleftarrows}}\mathrm{ADP.Pi}\underset{k_{-5}}{\overset{k_5}{\rightleftarrows}}\mathrm{ADP}$, where we assumed that there exists a rate limiting intermediate state for ADP release, denoted by ADP*, and the transition from ADP to ADP* may accompany the power stroke [21,27,40,41], i.e., the rotation of neck domain from Fig. 2(b) to (a). Thus the transition rate k_{-1} should be much smaller than the rate k_1 and, for simplicity of analysis, we can neglect this transition from ADP* to ADP. In addition, we can also neglect the transition from ADP to ADP. Pi as no Pi is assumed to be present and neglect the much slow transition from ATP to Empty states and the much slow

transition from ADP.Pi to ATP states [22]. Thus the above scheme becomes

$$\mathrm{ADP}\xrightarrow{k_1}\mathrm{ADP}^*\underset{k_{-2}}{\overset{k_2}{\rightleftarrows}}\mathrm{Empty}\xrightarrow{k_3}\mathrm{ATP}\xrightarrow{k_4}\mathrm{ADP.Pi}\xrightarrow{k_5}\mathrm{ADP}. \tag{5}$$

The transition rates k_i ($i=1, 2, 4, 5$) are independent of [ATP] and [ADP], k_3 is [ATP] dependent, i.e., $k_3=k_T$[ATP], and k_{-2} is [ADP] dependent, i.e., $k_{-2}=k_D$[ADP].

When a force, F, which is opposite to the moving direction, is acted on the myosin head, the chemical reaction rates follow the kinetics of an enzymatic reaction, which is in the general Boltzmann form [42,43]

$$k_i=\frac{k_{i0}(1+A_i)}{1+A_i\exp(F\delta_i/k_BT)}\qquad(i=1,2,4,5,T,D). \tag{6}$$

When $A_i=0$, $k_i=k_{i0}$ is load independent and, when $A_i\gg 1$, Eq. (6) is reduced to $k_i=k_{i0}\exp(-F\delta_i/k_BT)$. From our model, the force F acted on the bound trailing head of myosin-VI in rigor state (Fig. 4(a)) is

$$F=F_{\mathrm{load}}-F_x. \tag{7}$$

From the model we presented in Section 3, the dwell period of myosin-VI corresponds to that in which a given myosin head is bound to actin in ADP and Empty (or nucleotide-free) states (i.e., Fig. 4(d) and (a)). Thus, from scheme (5), the pathway for the dwell period corresponds to the following scheme for the actin-bound head,

$$\mathrm{ADP}\xrightarrow{k_1}\mathrm{ADP}^*\underset{k_{-2}}{\overset{k_2}{\rightleftarrows}}\mathrm{Empty}\xrightarrow{k_3}\mathrm{ATP}. \tag{8}$$

For convenience of writing, we denote the probabilities of finding the actin-bound myosin head in ADP, ADP*, Empty, and ATP states by D, D^*, E, and T, respectively. Then from scheme (8), they are described by the following differential equations

$$\frac{dD}{dt}=-k_1D, \tag{9a}$$

$$\frac{dD^*}{dt}=k_1D+k_{-2}E-k_2D^*, \tag{9b}$$

$$\frac{dE}{dt}=k_2D^*-(k_{-2}+k_3)E, \tag{9c}$$

$$\frac{dT}{dt}=k_3E. \tag{9d}$$

Solving Eqs. (9a)–(9d) with initial conditions at $t=0$: $D(0)=1$, $D^*(0)=0$, $E(0)=0$ and $T(0)=0$, we obtain the probability density for dwell time, $f(t)=dT/dt$, as

$$f(t)=\frac{k_1k_2k_3}{2b}\times\left(\frac{e^{(a+b)t}}{k_1+a+b}-\frac{e^{(a-b)t}}{k_1+a-b}+\frac{2be^{-k_1t}}{(k_1+a+b)(k_1+a-b)}\right), \tag{10}$$

where $a=-(k_2+k_{-2}+k_3)/2$ and $b=(a^2-k_2k_3)^{1/2}$. From Eq. (10), the mean dwell time is obtained as

$$\tau_{\mathrm{dwell}}=\frac{1}{k_1}+\frac{1}{k_2}+\frac{1}{k_3}+\frac{k_{-2}}{k_2k_3} \tag{11}$$

In the case of no ADP, τ_{dwell} can be written as

$$\tau_{\mathrm{dwell}}=\frac{k_{\mathrm{D-release}}/k_T+[\mathrm{ATP}]}{k_{\mathrm{D-release}}[\mathrm{ATP}]}, \tag{12}$$

where $k_{\mathrm{D\text{-}release}}=k_1k_2/(k_1+k_2)$ is the mean ADP-release rate. Note that Eq. (12) has the Michaelis–Menten form. Eqs. (6), (10) and (11) constitute the basis for our theoretical approach to the kinetics of myosin molecules and we will use them to make all the calculations in the following sections.

6. Results for dwell time

The values of parameters for myosin-VI are shown in Table 1. The value of F_x in rigor state of Fig. 4(a) is taken as $F_x=1$ pN. Note that this value of F_x in rigor state is smaller than that during the moving period as shown in Fig. 4(b). This is because in Fig. 4(a) F_x is the net force determined mainly by the binding force from binding sites near site (II) and that from binding sites near site (I), while in Fig. 4(b) F_x is the force determined mainly by the binding force from binding sites near site (II) and that from binding sites near site (I) is nearly zero. From Table 1, the value of ATP-binding rate $k_T=20\ \mathrm{mM^{-1}\ s^{-1}}$ is consistent with the measured value of $\sim 18\ \mathrm{mM^{-1}\ s^{-1}}$ [44] for truncated single-headed myosin-VI by bulk assays. From the values of k_{10} and k_{20}, the obtained mean ADP-release rate $k_{\mathrm{D\text{-}release}}=k_{10}k_{20}/(k_{10}+k_{20})=3.5\ \mathrm{s^{-1}}$ is consistent with the measured value of $\sim 5.5\ \mathrm{s^{-1}}$ [44] for truncated single-headed myosin-VI by bulk assays.

At saturating [ATP]=2 mM, $k_3=k_T$[ATP]$\to\infty$, the dwell time depends only on ADP-release activity and the dwell-time distribution $f(t)$ in Eq. (10) is reduced to a two-exponential form, $f(t)=k_1k_2(k_2-k_1)^{-1}[\exp(-k_1t)-\exp(-k_2t)]$. This is consistent with the experimental result (Fig. 3 in Ref. [12]). The calculated k_1 and k_2 versus loads by using Eq. (10) are shown in Fig. 6(a), where the data points are taken from the experimental results [12]. In Fig. 6 (b) we show the calculated mean dwell time versus load for different ATP concentrations by using Eqs. (6) and (11). Note that, at saturating [ATP], the inverse of mean dwell time versus load also follows a form similar to k_2, i.e., $\tau_{\mathrm{dwell}}^{-1}=k_0(1+A)/[1+A\exp(F\delta_2/k_BT)]$, with $k_0=k_{10}k_{20}/(k_{10}+k_{20})=3.5\ \mathrm{s^{-1}}$ and $A=A_2/[1+(1+A_2)k_{20}/k_{10}]\approx 1\times 10^{-7}$.

In Fig. 7(a), we show the calculated mean dwell time as a function of ATP concentration at different loads by using Eqs.

Table 1
Values of parameters for myosin-VI

i	k_{i0}	A_i	δ_i
1	$5\ \mathrm{s^{-1}}$	0	
2	$11.66\ \mathrm{s^{-1}}$	3.31×10^{-7}	61.5 nm
T	$20\ \mathrm{mM^{-1}\ s^{-1}}$	$\gg 1$	3.6 nm
D	$46.8\ \mu\mathrm{M^{-1}\ s^{-1}}$	$\gg 1$	−5 nm

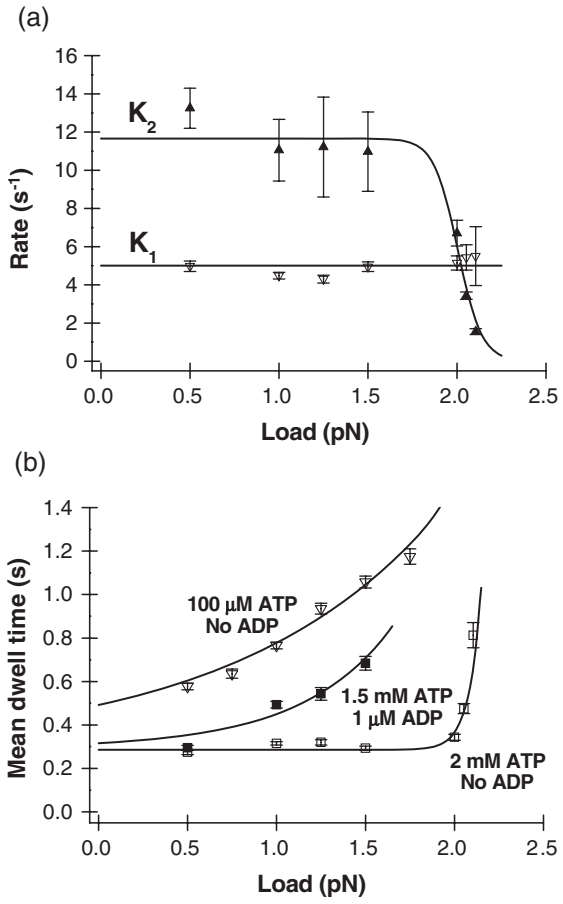

Fig. 6. (a) Dependence of k_1 and k_2 on load at saturating [ATP] of 2 mM. (b) Dependence of mean dwell time on load at different [ATP] and [ADP]. Solid lines are calculated results and data points are experimental results [12].

(6) and (11). Fig. 7(b) corresponds to the ATP-binding rate versus load calculated by using Eq. (6), and Fig. 7(c) corresponds to the ADP-concentration dependence of mean dwell time. As mentioned above, at saturating [ATP] and no ADP, the dwell-time distribution $f(t)$ has a two-exponential form. However, as seen from Eq. (10), the dwell-time distribution $f(t)$ at low [ATP] has a three-exponential form. We numerically verified that the three-exponential form of $f(t)$ at all ATP concentrations can be fitted well by the two-exponential form,

$$f'(t) = \frac{k_1' k_2'}{k_2' - k_1'} [\exp(-k_1' t) - \exp(-k_2' t)], \tag{13}$$

if, as did in Ref. [12], we fix $k_1' = 4.1\ s^{-1}$ and vary k_2'. The fitted parameter values of k_2' as a function of [ATP] at $F_{load} = 1$ pN are shown in Fig. 7(d) (filled rhombuses), where the unfilled triangular points are taken from the experimental results [12]. We see that the fitted values of k_2' are in good agreement with the experimental ones. It is interesting to note that k_2' versus [ATP] follows the Michaelis–Menten equation very well, i.e.,

$$k_2' = \frac{k_2[\mathrm{ATP}]}{k_2/k_T + [\mathrm{ATP}]}, \tag{14}$$

as shown by the line in Fig. 7(d), where k_2 and k_T are the values at $F_{load} = 1$ pN.

This is understood as follows: At saturating [ATP], k_2' becomes the same as k_2 and the [ATP] dependence of k_2' is only through the ATP binding. In fact, from Eq. (13), the mean dwell time can be obtained as $\tau = (k_1' + k_2')/(k_1' k_2')$. By comparing it with Eq. (12), we see that, if we let $k_1' = k_1$, then we obtain Eq. (14).

Note that all the above calculated results are using the same parameters given in Table 1 and the calculated results show excellent agreement with the experimental results available.

7. Discussion

The present hand-over-hand diffusing model shows that, during the processive movement of myosin-VI, a given point at one of its neck domains near the coiled coil is displaced in discrete steps with the mean size of ~36 nm. (Speaking more precisely, the displacement should be composed of two distributions with mean step sizes of ~32 and ~40 nm, respectively, see Fig. 4.) However, recent experiments on myosin-VI labeled with Cy3 or Cy5 fluorophore demonstrated that the given point moves in discrete steps with the mean size of ~55.2 nm [16]. We give the explanation to this discrepancy as follows: In the experiments, the stepping traces were measured at [ATP] = 40 μM, with the integration time of ~0.5 s [15,16]. From parameters given in Table 1 the mean dwell time of myosin-VI is ~0.5 s at [ATP] = 40 μM, which is nearly the same as the integration time. That implies that about half of the measured step sizes would have a mean value of ~36 nm and another half would have a mean value of ~72 nm that should be due to two successive steps. (Speaking more precisely, about half of the measured step sizes would follow two Gaussian distributions with peak values of ~32 and ~40 nm, while the other half would follow one Gaussian distribution with a peak value of ~72 nm.) Therefore, the mean measured step size would be ~54 nm, which is in agreement of the experimental one of 55.2 nm [16]. The distribution that is composed of two Gaussian distributions, i.e., $\frac{1}{2}\left[\frac{1}{\sqrt{\pi/2}S}\exp\left(-\frac{(x-36)^2}{2\times S^2}\right)+\frac{1}{\sqrt{\pi/2}S}\exp\left(-\frac{(x-72)^2}{2\times S^2}\right)\right]$, with $S = 15$ nm is shown in Fig. 8 (a), which shows good resemblance to Fig. 1(a) of Ref. [16]. Similarly, based on the present model, the measured step size of a given motor domain should follow the distribution that is composed of two Gaussian distributions with peak values of ~65 and ~72 nm. This gives the mean measured step size of ~68.5 nm, which is in agreement with the experimental one of ~63.3 nm [16]. The distribution that is composed of two Gaussian distributions, i.e., $\frac{1}{2}\left[\frac{1}{\sqrt{\pi/2}S}\exp\left(-\frac{(x-65)^2}{2\times S^2}\right)+\frac{1}{\sqrt{\pi/2}S}\exp\left(-\frac{(x-72)^2}{2\times S^2}\right)\right]$ with $S = 15$ nm is shown in Fig. 8(b). This also shows good resemblance to Fig. 1(b) of Ref. [16]. In addition, it is interesting to note that, based on the present model, the myosin-VI is displaced in discrete steps with the mean size of ~36 nm under no or low load. This is also in good agreement with various experimental results by using other methods with high temporal resolutions [9,12,13]. As we mentioned in Section 3, the present model gives the mean inter-head distance of ~29 nm that also shows very well agreement with

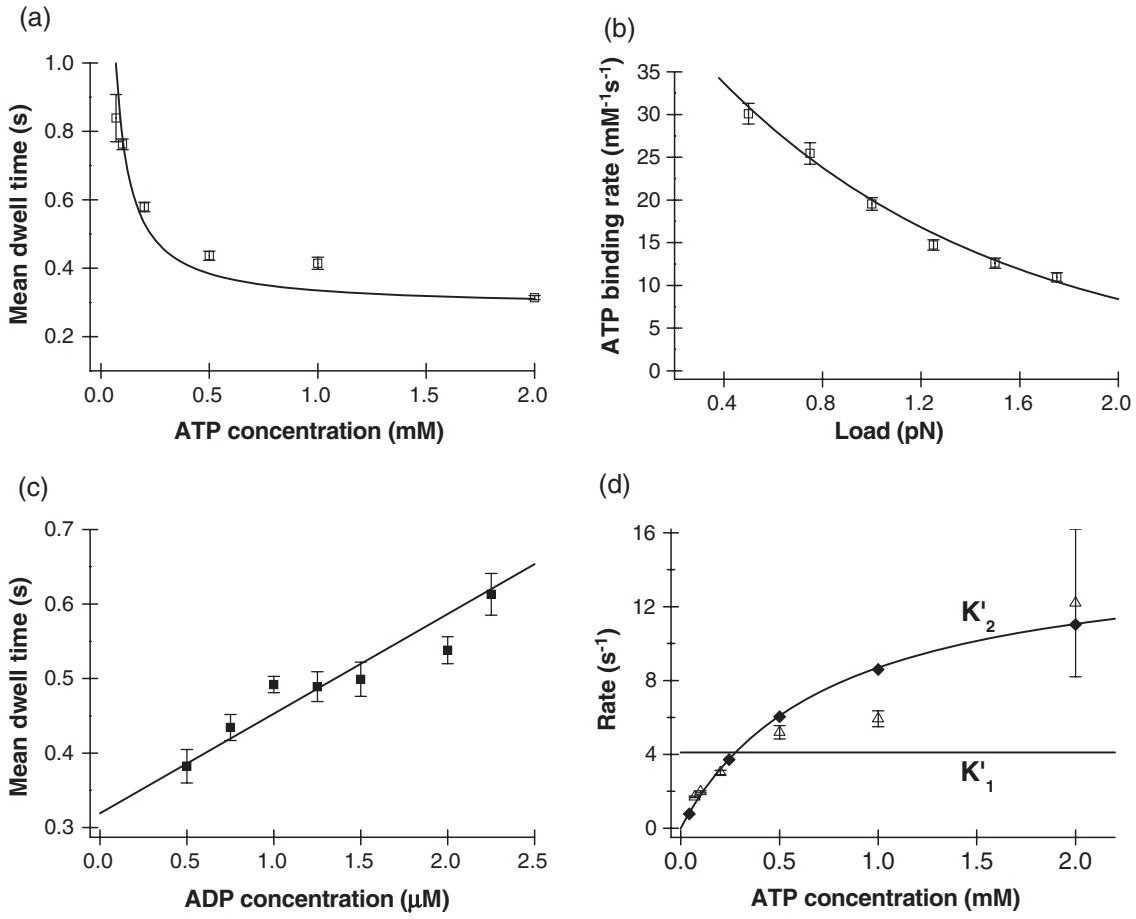

Fig. 7. (a) Mean dwell time as a function of [ATP] at 1 pN load. (b) ATP-binding rate versus load. (c) Mean dwell time as a function of [ADP] at 1 pN load. Solid lines in (a)–(c) are calculated results and data points are experimental results [12]. (d) k_1' and k_2' as a function of [ATP] at 1 pN load. Filled rhombuses are fitted values of k_2' by fixing k_1' and the solid line is calculated from Eq. (13). Unfilled triangles are experimental results [12].

the experimental result of ~29.3 nm [38]. Therefore, the various distances or mean step sizes determined by using different methods are explained.

According to the present hand-over-hand diffusing mechanism, during the moving period of myosin-VI in one step both heads are detached from actin. It is thus easy for myosin-VI to diffuse away from (or release) actin and it will not have a long run length. By contrast, because during the moving period of myosin-V and conventional kinesin in one step one head remains bound strongly to their tracks (actin and microtubule, respectively), thus it is not easy for them to diffuse away from their tracks. These results are indeed supported by experiments. For example, from the measured mean run length of 226 nm [8], myosin-VI can take about 226/36 nm ≈ 6.3 steps before releasing actin. By contrast, myosin-V can take at least 40−50 steps [45] and kinesin can take about 100 steps [46] before releasing their tracks.

As we mentioned in the Introduction, two other models have been proposed in the literature. One is the model based on biased Brownian motion, where the movement of myosin-VI is realized by biased thermal diffusion of its heads along actin [9]. However, in this model, how the interaction potential between the myosin head and actin is biased is difficult to imagine from the structure of actin. Another prevailing model is the modification of the lever-arm model [8,12,14–16]. This model presumes a step consisting of a working stroke of the short lever arm followed by a diffusive search. The working stroke provides part of the step size and imparts directionality while the diffusive search allows the leading head to find further actin-binding sites. This proposal assumes that, during the motile cycle of myosin-VI along actin, the region immediately following the IQ motif (the proximal tail) might come apart more than 24 nm so that the leading head (in ADP.Pi state) can also bind to actin [14]. In rigor state for this model there should exist an internal elastic force, F_0, acted on the two heads, with the trailing head being pulled forward. In order to move forward after ATP binding to the trailing head, this internal force F_0 should be at least equal to the stall force of ~2.8 pN [8]. Thus the force acted on the trailing head in Eq. (6) should be $F = F_{\text{load}} - F_0$. If we use this F (where $F_0 = 2.8$ pN) to fit the experimental data given in Figs. 6 and 7, we will obtain the mean ATP-binding rate $k_T = 4.25\ \text{mM}^{-1}\ \text{s}^{-1}$ and the mean ADP-release rate $k_{\text{D-release}} \approx 10^{-4}\ \text{s}^{-1}$ under $F = 0$. This ATP-binding rate is more than four times smaller than the measured value of ~18 $\text{mM}^{-1}\ \text{s}^{-1}$ and the ADP-release rate is more than *5 orders of magnitude* smaller than the measured value of ~5.5 s^{-1} for truncated single-headed myosin-VI by bulk assays [44]. In addition, because the farther away the binding site on which the leading

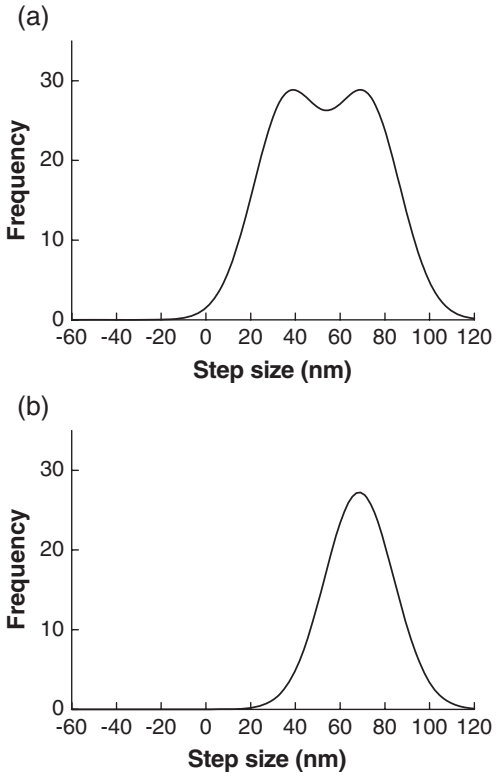

Fig. 8. Calculated step-size distributions for a given point at one of the neck domains near the coiled coil (a) and for a given point at one of the motor domains (b) during the processive movement of myosin-VI at [ATP]=40 μM.

head will bind, the larger the internal elastic force F_0 needed to overcome by Brownian diffusion. Thus it is expected that, even under no load, the mean step size would be smaller than the half-repeat distance of actin (d=36 nm) and the step-size distribution will not be symmetric but decline sharply beyond the peak. These are obviously inconsistent with the measured mean step size of ~36 nm under no or low load [9,12,13] and the measured nearly Gaussian distribution of step sizes [9,15].

An interesting experimental result for myosin-VI is that both the step size and the frequency of backward stepping relative to forward stepping do not change significantly with varying load under stall force [12]. Based on the present model, this can be explained as follows: Since upon the detachment of the trailing head the leading head will bind to actin immediately, which means a very short diffusing time, thus the load would have little effect on the displacement of the myosin from the moment of detachment of the trailing head to the moment of binding of the leading head. Therefore, the variation of the load will have little effect on both the step size and the frequency of backward stepping relative to forward stepping. Note here that, in the present model, the stall force corresponds to the load under which the mean dwell time, i.e., the ADP-release time, becomes infinity. This is different from the case of kinesin, where the stall force corresponds to the load under which the unattached head becomes stalled [23,43]. However, according to a previous model [14], because of the flexible portion immediately following the IQ motif, the frequency for the free head to diffuse 24 nm will decrease significantly with increasing backward load. Thus the load would have significant effect on both the step size of forward stepping and the frequency of backward stepping relative to forward stepping, which is inconsistent with the experimental result [12].

The present model can also be applicable to mutant myosin-V with its neck domain truncated to only one-sixth of the native length [47]. Similar to native myosin-V [17], the equilibrium conformation of mutant myosin-V is shown in Fig. 9, with one head in ADP or nucleotide-free state and the other one in ADP.Pi state. Note that the orientation between the neck domain and the motor domain for mutant myosin-V is opposite to that for myosin-VI, thus resulting in the opposite moving directions along actin for the two motors. However, the similar hand-over-hand diffusing mechanism for the two motors will result in the similar dynamical behaviors. Therefore, the mutant myosin-V also moves with a wide step-size distribution and an average step size of ~36 nm, but towards the barbed (plus) end of actin. These results show good agreement with the experimental results [47]. It is important to note that, in rigor state of mutant myosin-V (Fig. 9), the unbound head is nearly positioned near the middle point between binding sites (I) and (II). Thus after ATP binding to the bound nucleotide-free head, although there exists a net force F_x pointed towards the barbed end, which drives mutant myosin-V moving to binding site (II), its magnitude is smaller than that for myosin-VI. This gives a smaller stall force and thus a larger ratio of backward stepping relative to forward stepping for mutant myosin-V than for myosin-VI. This is in agreement with the experimental results for mutant myosin-V, with stall force smaller than 1.8 pN and ratio between backward and forward steppings of ~1:10 [47], and for myosin-VI, with mean stall force of 2.8 pN and ratio of ~ 4:100 [8,12]. Moreover, in rigor state of mutant myosin-V (Fig. 9), the vertical distance of the unbound head from actin is larger than that of myosin-VI in rigor state (Fig. 3(c)). This thus gives the force F_y for mutant myosin-V to be smaller than myosin-VI. Therefore, the maximum number of run steps for mutant myosin-V (3 steps) [47] is smaller than myosin-VI (with mean 6.3 run steps) [8].

In Section 3, for convenience of writing, we assume that the power stroke is occurred by accompanying the release of Pi, i.e., the transition of ADP.Pi→ADP. In fact, the power stroke may have occurred by accompanying the transition of ADP→ADP*, as discussed in Section 5. Both cases give the same results in our analysis presented up to now. If the transition of ADP→ADP* induces the power stroke, from Fig. 4 we note that there exist

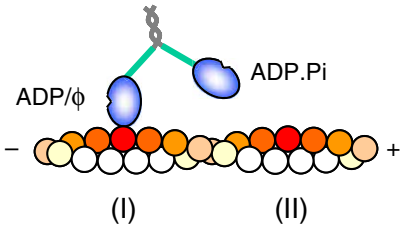

Fig. 9. Equilibrium conformation of mutant myosin-V (its neck domains truncated to only one IQ motif) with one head in ADP or nucleotide-free (ϕ) state and the other one in ADP.Pi state. Note that the orientation of its neck domain relative to the motor domain is opposite to that for myosin-VI.

two conformations during the dwell period: One is shown in Fig. 4(a) and the other one is shown in Fig. 4(c). It is interesting to note that Nishikawa et al. [9] have studied the actin binding behaviors of myosin-VI in an assay buffer containing ATP. They have observed that many of the myosin-VI molecules bind with a single head to actin in conformations much resembling the conformation as shown in Fig. 4(c).

In summary, we proposed a hand-over-hand diffusing model for dimeric myosins with short neck domains. Using this model, we study in detail various dynamical behaviors of myosin-VI such as the step-size distribution, dwell-time distributions and mean dwell time at various ATP and ADP concentrations and under various loads. The theoretical results show good agreement with the previous experimental results. Finally, we would like to mention that, according to the present model, it is predicted that only half of Pi is released quickly while the other half cannot be released or is released very slowly after mixing ADP.Pi–myosin-VI complex with actin, which needs to be tested in future experiment.

Acknowledgements

This work was supported by the National Natural Science Foundation of China.

References

[1] F. Buss, J.P. Luzio, J. Kendrick-Jones, Myosin VI, an actin motor for membrane traffic and cell migration, Traffic 3 (2002) 851–858.
[2] E.R. Geisbrecht, D.J. Montell, Myosin VI is required for E-cadherin-mediated border cell migration, Nat. Cell Biol. 4 (2002) 616–620.
[3] F. Buss, G. Spudich, J. Kendrick-Jones, Myosin VI: cellular functions and motor properties, Annu. Rev. Cell Dev. Biol. 20 (2004) 649–676.
[4] H. Millo, K. Leaper, V. Lazou, M. Brownes, Myosin VI plays a role in cell–cell adhesion during epithelial morphogenesis, Mech. Dev. 121 (2004) 1335–1351.
[5] I. Lister, R. Roberts, S. Schmitz, M. Walker, J. Trinick, C. Veigel, F. Buss, J. Kendrick-Jones, Myosin VI: a multifunctional motor, Biochem. Soc. Trans. 32 (2004) 685–688.
[6] A.L. Wells, A.W. Lin, L.-Q. Chen, D. Safer, S.M. Cain, T. Hasson, B.O. Carragher, R.A. Milligan, H.L. Sweeney, Myosin VI is an actin-based motor that moves backwards, Nature 401 (1999) 505–508.
[7] I. Lister, S. Schmitz, M. Walker, J. Trinick, F. Buss, C. Veigel, J. Kendrick-Jones, A monomeric myosin VI with a large working stroke, EMBO J. 23 (2004) 1729–1738.
[8] R.S. Rock, S.E. Rice, A.L. Wells, T.J. Purcell, J.A. Spudich, H.L. Sweeney, Myosin VI is a processive motor with a large step size, Proc. Natl. Acad. Sci. U. S. A. 98 (2001) 13655–13659.
[9] S. Nishikawa, K. Homma, Y. Komori, M. Iwaki, T. Wazawa, A.H. Iwane, J. Saito, R. Ikebe, E. Katayama, T. Yanagida, M. Ikebe, Class VI myosin moves processively along actin filaments backward with large steps, Biochem. Biophys. Res. Commun. 290 (2002) 311–317.
[10] K. Homma, M. Yoshimura, J. Saito, R. Ikebe, M. Ikebe, The core of the motor domain determines the direction of myosin movement, Nature 412 (2001) 831–834.
[11] J. Ménétrey, A. Bahloul, A.L. Wells, C.M. Yengo, C.A. Morris, H.L. Sweeney, A. Houdusse, The structure of the myosin VI motor reveals the mechanism of directionality reversal, Nature 435 (2005) 779–785.
[12] D.A. Altman, H.L. Sweeney, J.A. Spudich, The mechanism of myosin VI translocation and its load-induced anchoring, Cell 116 (2004) 737–749.
[13] M.Y. Ali, K. Homma, A.H. Iwane, K. Adachi, H. Itoh, K. Kinosita Jr., T. Yanagida, M. Ikebe, Unconstrained steps of myosin VI appear longest among known molecular motors, Biophys. J. 86 (2004) 3804–3810.
[14] R.S. Rock, B. Ramamurthy, A.R. Dunn, S. Beccafico, B.R. Rami, C. Morris, B.J. Spink, C. Franzini-Armstrong, J.A. Spudich, H.L. Sweeney, A flexible domain is essential for the large step size and processivity of myosin VI, Mol. Cell 17 (2005) 603–609.
[15] Z. Ökten, L.S. Churchman, R.S. Rock, J.A. Spudich, Myosin VI walks hand-over-hand along actin, Nat. Struct. Mol. Biol. 11 (2004) 884–887.
[16] A. Yildiz, H. Park, D. Safer, Z. Yang, L.-Q. Chen, P.R. Selvin, H.L. Sweeney, Myosin VI steps via a hand-over-hand mechanism with its lever arm undergoing fluctuations when attached to actin, J. Biol. Chem. 279 (2004) 37223–37226.
[17] P. Xie, S.-X. Dou, P.-Y. Wang, Model for processive movement of myosin V and myosin VI, Chin. Phys. 14 (2005) 744–752.
[18] M.A. Geeves, K.C. Holmes, Structural mechanism of muscle contraction, Annu. Rev. Biochem. 68 (1999) 687–728.
[19] S. Highsmith, Lever arm model of force generation by actinmyosin–ATP, Biochemistry 38 (1999) 9791–9797.
[20] A. Houdusse, H.L. Sweeney, Myosin motors: missing structures and hidden springs, Curr. Opin. Struct. Biol. 11 (2001) 182–194.
[21] J.A. Spudich, The myosin swinging cross-bridge model, Nat. Rev., Mol. Cell. Biol. 2 (2001) 387–392.
[22] M.A. Geeves, R. Fedorov, D.J. Manstein, Molecular mechanism of actomyosin-based motility, CMLS, Cell. Mol. Life Sci. 62 (2005) 1462–1477.
[23] P. Xie, S.-X. Dou, P.-Y. Wang, Model for kinetics of wild-type and mutant kinesins, Biosystems 84 (2006) 24–38.
[24] C. Veigel, F. Wang, M.L. Bartoo, J.R. Sellers, J.E. Molloy, The gated gait of the processive molecular motor, myosin V, Nat. Cell Biol. 4 (2002) 59–65.
[25] E. Prochniewicz, T.F. Walseth, D.D. Thomas, Structural dynamics of actin during active interaction with myosin: different effects of weakly and strongly bound myosin heads, Biochemistry 43 (2004) 10642–10652.
[26] H.D. White, B. Belknap, M.R. Webb, Kinetics of nucleoside triphosphate cleavage and phosphate release steps by associated rabbit skeletal actomyosin, measured using a novel fluorescent probe for phosphate, Biochemistry 36 (1997) 11828–11836.
[27] H.L. Sweeney, A. Houdusse, The motor mechanism of myosin V: insights for muscle contraction, Philos. Trans. R. Soc. Lond., B 359 (2004) 1829–1841.
[28] N.B. Becker, S.M. Altmann, T. Scholz, J.K.H. Hörber, E.H.K. Stelzer, A. Rohrbach, Three-dimensional bead position histograms reveal single-molecule nanomechanics, Phys. Rev., E 71 (2005) 021907.
[29] R.A. Mendelson, P.H. Cheung, Intrinsic segmental flexibility of the S-1 moiety of myosin using single-headed myosin, Biochemistry 17 (1978) 2139–2148.
[30] S. Ishiwata, K. Kinosita Jr., H. Yoshimura, A. Ikegami, Rotational motion of myosin heads in myofibril studied by phosphorescence anisotropy decay measurements, J. Biol. Chem. 262 (1987) 8314–8317.
[31] T. Sakamoto, F. Wang, S. Schmitz, Y. Xu, Q. Xu, J.E. Molloy, C. Veigel, J. R. Sellers, Neck length and processivity of myosin V, J. Biol. Chem. 278 (2003) 29201–29207.
[32] F. Wang, L. Chen, O. Arcucci, E.V. Harvey, B. Bowers, Y. Xu, J.A. Hammer III, J.R. Sellers, Effect of ADP and ionic strength on the kinetic and motile properties of recombinant mouse myosin V, J. Biol. Chem. 275 (2000) 4329–4335.
[33] E. Katayama, Quick-freeze deep-etch electron microscopy of the actin-heavy meromyosin complex during the in vitro motility assay, J. Mol. Biol. 278 (1998) 349–367.
[34] K. Kinosita Jr., M.Y. Ali, K. Adachi, K. Shiroguchi, H. Itoh, How two-foot molecular motors may walk, Adv. Exp. Med. Biol. 565 (2005) 205–219.
[35] F. Kozielski, S. Sack, A. Marx, M. Thormahlen, E. Schonbrunn, V. Biou, A. Thompson, E.-M. Mandelkow, E. Mandelkow, The crystal structure of dimeric kinesin and implications for microtubule-dependent motility, Cell 91 (1997) 985–994.
[36] Y. Li, J.H. Brown, L. Reshetnikova, A. Blazsek, L. Farkas, L. Nyitray, C. Cohen, Visualization of an unstable coiled coil from the scallop myosin rod, Nature 424 (2003) 341–345.
[37] M. Terrak, G. Rebowski, R.C. Lu, Z. Grabarek, R. Dominguez, Structure of the light chain-binding domain of myosin V, Proc. Natl. Acad. Sci. U. S. A. 102 (2005) 12718–12723.

[38] H. Balci, T. Ha, H.L. Sweeney, P.R. Selvin, Interhead distance in myosin VI via SHRIMP supports a hand-over-hand model with a long lever arm, Biophys. J. 89 (2005) 413–417.
[39] W. Steffen, D. Smith, R. Simmons, J. Sleep, Mapping the actin filament with myosin, Proc. Natl. Acad. Sci. U. S. A. 98 (2001) 14949–14954.
[40] R. Cooke, Actomyosin interaction in striated muscle, Physiol. Rev. 77 (1997) 671–697.
[41] Y.E. Goldman, Wag the tail: structural dynamics of actomyosin, Cell 93 (1998) 1–4.
[42] M.D. Wang, M.J. Schnitzer, H. Yin, R. Landick, J. Gelles, S.M. Block, Force and velocity measured for single molecules of RNA polymerase, Science 282 (1998) 902–907.
[43] P. Xie, S.-X. Dou, P.-Y. Wang, Mechanism for unidirectional movement of kinesin, Chin. Phys. 14 (2005) 734–743.
[44] E.M. De La Cruz, E.M. Ostap, H.L. Sweeney, Kinetic mechanism and regulation of myosin VI, J. Biol. Chem. 276 (2001) 32373–32381.
[45] A.D. Mehta, R.S. Rock, M. Rief, J.A. Spudich, M.S. Mooseker, R.E. Cheney, Myosin-V is a processive actin-based motor, Nature 400 (1999) 590–593.
[46] M.J. Schnitzer, K. Visscher, S.M. Block, Force production by single kinesin motors, Nat. Cell Biol. 2 (2000) 718–723.
[47] H. Tanaka, K. Homma, A.H. Iwane, E. Katayama, R. Ikebe, J. Saito, T. Yanagida, M. Ikebe, The motor domain determines the large step of myosin-V, Nature 415 (2002) 192–195.
[48] M.L. Walker, S.A. Burgess, J.R. Sellers, F. Wang, J.A. Hammer, J. Trinick, P.J. Knight, Two-headed binding of a processive myosin to F-actin, Nature 405 (2000) 804–807.